NIH Public Access
Author Manuscript
Pharm Res. Author manuscript; available in PMC 2014 May 01.

Published in final edited form as:
Pharm Res. 2013 May ; 30(5): . doi:10.1007/s11095-013-0980-0.

Importance of Peptide Transporter 2 on the Cerebrospinal Fluid Efflux Kinetics of Glycylsarcosine Characterized by Nonlinear Mixed Effects Modeling

Yeamin Huh,
Department of Pharmaceutical Sciences, University of Michigan, Ann Arbor, Michigan 48109, USA

Scott M. Hynes,
Global PK/PD and Pharmacometrics, Lilly Research Laboratories, Lilly Corporate Center, Indianapolis, Indiana, USA

David E. Smith, and
Department of Pharmaceutical Sciences, University of Michigan, Ann Arbor, Michigan 48109, USA

Meihua R. Feng
Department of Pharmaceutical Sciences, University of Michigan, Ann Arbor, Michigan 48109, USA

Meihua R. Feng: fengmr@umich.edu

Abstract

Purpose—To develop a population pharmacokinetic model to quantitate the distribution kinetics of glycylsarcosine (GlySar), a substrate of peptide transporter 2 (PEPT2), in blood, CSF and kidney in wild-type and PEPT2 knockout mice.

Methods—A stepwise compartment modeling approach was performed to describe the concentration profiles of GlySar in blood, CSF, and kidney simultaneously using nonlinear mixed effects modeling (NONMEM). The final model was selected based on the likelihood ratio test and graphical goodness-of-fit.

Results—The profiles of GlySar in blood, CSF, and kidney were best described by a four-compartment model. The estimated systemic elimination clearance, volume of distribution in the central and peripheral compartments were 0.236 vs 0.449 ml/min, 3.79 vs 4.75 ml, and 5.75 vs 9.18 ml for wild-type *versus* knockout mice. Total CSF efflux clearance was 4.3 fold higher for wild-type compared to knockout mice. NONMEM parameter estimates indicated that 77% of CSF efflux clearance was mediated by PEPT2 and the remaining 23% was mediated by the diffusional and bulk clearances.

Conclusions—Due to the availability of PEPT2 knockout mice, we were able to quantitatively determine the significance of PEPT2 in the efflux kinetics of GlySar at the blood-cerebrospinal fluid barrier.

© Springer Science+Business Media New York 2013
Correspondence to: Meihua R. Feng, fengmr@umich.edu.

NIH-PA Author Manuscript
NIH-PA Author Manuscript
NIH-PA Author Manuscript

NIH-PA Author Manuscript

NIH-PA Author Manuscript

NIH-PA Author Manuscript

Keywords

cerebrospinal fluid; nonlinear mixed effects modeling; peptide transporter 2; population pharmacokinetics

INTRODUCTION

The blood-cerebrospinal fluid barrier (BCSFB) is formed by choroid plexus epithelial cells of the ventricles and cells of the arachnoid membrane that cover the surface of the brain. Similar to the blood–brain barrier (BBB), the BCSFB protects the central nervous system (CNS) from unwanted toxic compounds in the blood supply to maintain a constant extracellular environment for normal brain function (1,2). The BCSFB has several advantages for drug delivery to the brain. First, because of the basolateral infoldings and numerous apical microvilli, choroid plexus epithelial cells have a large surface area for exchange of drug molecules. Second, the tight junctions linking choroid plexus epithelial cells are relatively weak compared to the BBB and, thus, the BCSFB has a relatively high permeability (3). Third, the BCSFB allows direct access to the ventricles, ependyma and subependymal tissue, leptomeninges, outerlayers of pial vessels, and perivascular spaces (4,5). Therefore, the BCSFB can be a useful target for drug delivery to the brain in several CNS disease states.

Choroid plexuses possess a variety of transport proteins that act as gate keepers for the inward and outward movement of molecules across the BCSFB. Inwardly directed basolateral transport proteins can facilitate the entry of molecules (e.g., nutrients) into the CSF, whereas outwardly directed apical transport proteins can facilitate the elimination of undesired molecules (e.g., drugs and CSF–born endogenous metabolites) into the blood. The main drug transporters in choroid plexus belong to two superfamilies, the solute carrier (SLC) family including OAT1–3, OATP3 and PEPT2, and the ATP–binding cassette (ABC) carrier family including P–gp and MRP1. The membrane expression of SLC and ABC transporters are polarized and, thereby, allow for efficient movement of drug substrates across the BCSFB (1,6). Peptide transporter 2 (PEPT2) is abundantly expressed at the apical surface of choroid plexus epithelia and plays an important role in the efflux of substrate molecules from CSF to blood.

PEPT2 belongs to the proton–coupled oligopeptide transporter (POT) family and is responsible for the cellular uptake of di- and tripeptides in the organism *via* an inwardly directed electrochemical proton gradient. There are four members of the POT family in mammals: PEPT1, PEPT2, PHT1 and PHT2. Compared to PEPT1, which is a low-affinity and high-capacity transporter, PEPT2 is characterized as a high-affinity and low-capacity transporter (7). PEPT2 is predominantly localized in apical membrane of epithelium in the kidney proximal tubule and brain choroid plexus. It also has been detected in the lung, mammary gland and other tissues of brain (astrocytes, sub-ependymal cells, and ependymal cells). It is generally believed that PEPT2 is responsible for the reabsorption of small peptides and peptide-like drugs in kidney (8-10), as well as neuropeptide homeostasis in choroid plexus (11-13). Especially in choroid plexus of brain, PEPT2 pumps out peptidomemetic drugs (i.e. cefadroxil) and neuropeptides (i.e. 5-aminolevulinic acid and L-kyotorphin) from CSF into the blood and thereby restricts the delivery of these substrate molecules to the CNS (14-16).

Description of CSF pharmacokinetics is important in predicting and understanding pharmacologic actions of CNS drugs (17). In clinical studies, only limited CSF samples are available per subject because of both medical and ethical reasons, which allows large

NIH-PA Author Manuscript

NIH-PA Author Manuscript

NIH-PA Author Manuscript

variation of data in the study. Nonlinear mixed effects modeling (NONMEM) is especially useful in this case to address different sources of variability and to identify major origins of variability. Several studies have developed CSF pharmacokinetic models of drugs using NONMEM data analysis (17-20). Since several mechanisms including transport proteins are involved in the influx and efflux of drugs at the brain, quantifying the importance of each distribution mechanism helps us to adjust the dose to meet both the efficacy and safety concerns of CNS drugs. A NONMEM approach can also be a useful tool to parameterize the distribution mechanisms between blood and brain, and to quantatively analyze the importance of different transport proteins as compared to passive processes.

With this in mind, the aim of this study was to develop a population pharmacokinetic model to describe the distribution kinetics of glycylsarcosine (GlySar), a model PEPT2 substrate, at the BCSFB. Our laboratory developed PEPT2-deficient mice, which allows us to study the physiological and pharmacological importance of this transporter in the body (21). With the use of PEPT2 knockout mice, we developed a distribution kinetics model that incorporated PEPT2 expression level data and quantitatively analyzed the importance of PEPT2 in the efflux mechanism of GlySar at the BCSFB.

MATERIALS AND METHODS

The distribution kinetics of the PEPT2 substrate GlySar was assessed at the BCSFB using nonlinear mixed effects modeling (NONMEM) based on data generated previously in our laboratory (14). In brief, gender-matched wild-type and PEPT2 knockout mice (6–8 weeks old) were anesthetized with sodium pentobarbital and then administered 100 μl of [^{14}C]GlySar (5 μCi/mouse for labeled GlySar and a total dose of 0.05 μmol/g body weight for both labeled and unlabeled GlySar) by tail vein injection. Blood samples (5 μl) were obtained at 0.25, 1, 2, 5, 10, 20, 30, 45, and 60 min after the intravenous bolus *via* tail nicks. A CSF sample (~5 μl) was collected by inserting a 28-gauge needle into the cisterna magna after the end of sampling. The mouse was then decapitated, and choroid plexuses from lateral and fourth ventricles and whole kidney were harvested. To correct the tissue concentrations of GlySar for vascular space, [^{3}H]inulin (1 μCi/mouse) was administered intravenously 2 min before harvesting the tissues. Tissue samples were weighed and solubilized in 0.5 ml of 1 M hyamine hydroxide for 24 h at 37°C. After solubilization, tissue homogenates, CSF, and blood samples were mixed with Ecolite(+) liquid scintillation cocktail (MP Biomedicals) and the level of radioactivity was measured by a dual-channel liquid scintillation counter (Beckman LS 3801; Beckman Coulter, Fullerton, CA). Corrected tissue concentrations of Glysar ($C_{tissue,\ corr}$, nmol/g wet tissue) were calculated as

$$C_{tiss,corr} = C_{tiss} - V \times C_b \quad (1)$$

where C_{tiss} is the uncorrected GlySar tissue concentration (nmol/g), V is the blood volume (ml/g) determined as the inulin space of tissue samples estimated from inulin concentration in the final blood sample (22), and C_b is the GlySar blood concentration (nmol/ml).

To investigate time course changes of tissue distributions in choroid plexuses and kidney, the tissue samples were also harvested at preselected time points (2, 5, 15 min) after intravenous administration of [^{14}C]GlySar. [^{3}H]Inulin (1 μCi/mouse) was administered 2 min before harvesting the tissues to correct for the vascular space and all the tissues were processed as previously described.

Non-compartment Analysis of GlySar Pharmacokinetics in Blood

Blood concentration *versus* time curves of GlySar were initially fit to a non-compartmental model with a weighting factor of unity. Total systemic clearance (CL_s), volume of

NIH-PA Author Manuscript

NIH-PA Author Manuscript

NIH-PA Author Manuscript

distibution steady state (V_{ss}), terminal half-life ($t_{1/2}$), and mean residence time (MRT) were calculated using the standard methods by WinNonlin version 5.0.1 (Pharsignt Inc., Mountain View, CA).

Population Pharmacokinetic Modeling of GlySar in Blood, CSF, and Kidney

Population pharmacokinetic modeling was carried out using a nonlinear mixed effects modeling approach with NONMEM software, version 7 (ICON Development Solutions, MD, USA). A subroutine ADVAN6 TRANS1 and the first-order conditional estimation were used to build the compartment models throughout the modeling procedure. The best model was determined based on the likelihood ratio test using objective function values (OFV; the lowest value corresponds to the best model) and graphical goodness-of-fit. For nested models, reductions of OFV of at least 3.83 units corresponds to improved fits at $p < 0.05$. Graphical and statistical analysis was implemented using S-Plus 6.2 and R version 2.12.2.

Model Building—A stepwise compartmental model building approach was performed to describe the distribution kinetics of GlySar in the blood, CSF, and kidney. As an initial step, one-, two- and three- compartment models were compared for the Glysar blood concentration-time course after intravenous administration. Nonlinear elimination kinetics have been reported at high doses of PEPT2 substrates possibly associated with a saturation of the reabsorption process in the kidney mediated by PEPT2. Since we only used data in mice following a low dose of GlySar (0.05 mmol/kg), first-order elimination kinetics were assumed in our analysis. Modeling using log-transformed or non-transformed blood concentration data was evaluated and the compartment model with better residual plots was selected.

Once the pharmacokinetic model for blood concentration data was established, the model was extended to include a CSF compartment. It has been shown that PEPT2 is expressed in choroid plexus of the brain and plays a role in transporting drug substrates from CSF to blood (1). Since GlySar is a PEPT2 substrate, after it enters the brain, the dipeptide can be removed from the CSF of brain to blood by passive diffusion, CSF bulk flow, or active clearance mediated by PEPT2. Therefore, distribution kinetics between the blood and CSF compartments can be parameterized by the following equations (Fig. 1a):

$$\begin{aligned} \frac{dA_{CSF}}{dt} &= K_{in}A_C - K_{out}A_{CSF} \\ &= K_{13diff}\,A_C - (K_{31diff}+K_{bulk}+K_{active})\,A_{CSF} \\ &= \frac{CL_{diff}}{V_C}A_C - \frac{(CL_{diff}+CL_{bulk}+CL_{active})}{V_{CSF}}A_{CSF} \\ &= \frac{CL_{in}}{V_C}A_C - \frac{CL_{CSF\ effux}}{V_{CSF}}A_{CSF} \end{aligned} \quad (2)$$

where A_{CSF} is the amount of GlySar in CSF, A_c is the amount of GlySar in central blood, V_c is the volume of central compartment, V_{CSF} is the volume of CSF compartment, K_{in} and K_{out} are the inter-compartment rate constants describing GlySar transport between the blood and CSF, K_{diff}, K_{bulk} and K_{active} are distribution rate constants describing GlySar transport between blood and CSF mediated by passive diffusion, CSF bulk flow and PEPT2, respectively, CL_{diff} is the clearance mediated by passive diffusion, CL_{bulk} is the clearance mediated by CSF bulk flow, CL_{active} is the active clearance mediated by PEPT2, CL_{in} and $CL_{CSF\ efflux}$ are the inter-compartment clearances describing GlySar transport between the blood and CSF. CL_{bulk} was set to a physiological value of 0.325 μl/min in mouse (23). Since PEPT2 is absent in knockout mice, CL_{diff} can be estimated from the knockout animal data. After CL_{diff} was estimated in the model for knockout mice, it was fixed in the model for wild-type mice and the CL_{active} estimated in these animals. Using this stepwise model

NIH-PA Author Manuscript

NIH-PA Author Manuscript

NIH-PA Author Manuscript

building process, all parameters for the distribution kinetics between blood and CSF were estimated.

The final step was to incorporate a kidney compartment to the model and establish a full pharmacokinetic model, which describes all the distribution and elimination kinetics of blood, CSF and kidney. The estimated kinetic parameters between blood and CSF in the previous step were fixed in this model building process. Since GlySar is only eliminated by kidney, all tissue distribution reservoirs eventually entered the kidney and were eliminated from the body. The full pharmacokinetic model is presented in Fig. 1b and the distribution kinetics between the blood and kidney compartment was modeled as follows:

$$\frac{dA_{kidney}}{dt} = K_{14} A_C - K_{41} A_{kidney} - K_{40} A_{kidney} \approx \frac{CL_S}{V_C} A_C - K_{40} A_{kidney} \quad (3)$$

where A_{kidney} is the amount of GlySar in kidney, K_{14} is the distribution rate constant describing GlySar transport from blood to kidney, K_{41} is the distribution rate constant describing GlySar transport from kidney to blood, CL_s is the systemic clearance, and K_{40} is the rate constant describing GlySar elimination from the kidney. K_{41} is assumed to be zero in the model, since GlySar is completely renally excreted (14).

The inter-animal variability for the PK parameters was described by an exponential variance model using the following equation:

$$P_i = P_{pop} \exp(\eta_i) \quad (4)$$

where P_i is the parameter estimate for the ith animal, P_{pop} is the population estimate of the parameter for a typical animal, and η_i is the inter-animal variability representing the inter-animal difference between P_i and P_{pop}. The values of η_i are assumed to follow a normal distribution with mean of zero and variance ω^2. All parameters were tested for the necessity of including inter-animal variability. An additive error model was considered for the residual unexplained variability in the log transformed data of GlySar concentration.

Nonparametric Bootstrap Analysis—The stability of the final model was evaluated by non-parametric bootstrap analysis in which 1,000 bootstrap runs were performed using Wings for NONMEM (http://wfn.sourceforge.net). Each bootstrap sample was generated by sampling with replacement from the original sample and the new data set had the same size as the original data set. These 1,000 individual new data sets were fitted to the final model developed from the original data set and bootstrap parameter estimates were obtained from each bootstrap data set. The median, 5th, and 95th percentile of the parameter estimates were calculated from the successful bootstrap runs to obtain a 90% bootstrap confidence interval.

Visual Predictive Check—The final PK model was also evaluated by visual predictive checks with 1,000 data sets simulated by NONMEM using the parameter estimates of the final model. The median, 5th, and 95th percentiles of the simulated concentrations were calculated at each time point for the blood, CSF and kidney compartments, and visually checked to see if the intervals can cover the observed data points. The visual predictive check plots were generated using R version 2.12.2.

NIH-PA Author Manuscript

NIH-PA Author Manuscript

NIH-PA Author Manuscript

RESULTS

Different Pharmacokinetic Behavior of GlySar Between Wild-Type and PEPT2 Knockout Mouse

GlySar concentrations were significantly lower in the blood and kidney in knockout mice compared to wild-type animals, whereas the CSF concentrations were significantly higher in knockout mice (Fig. 2). GlySar pharmacokinetic parameters in blood were estimated by a non-compartmental analysis as summarized in Table I. The volume of distribution (V_{ss}) was slightly increased ($p < 0.001$) and total systemic clearance (CL_s) was increased by almost 2-fold ($p < 0.001$) in knockout mice. Meanwhile, the mean residence time (MRT) was significantly decreased in knockout animals ($p < 0.05$). Since PEPT2 is absent in knockout animals, these changes in GlySar disposition can be attributable to the deletion of PEPT2 functionality (14). Based on these findings, we decided to develop a model, which describes the distribution kinetics of GlySar in blood, CSF and kidney, and to quantify the importance of PEPT2 in the distribution kinetics of GlySar.

Population Pharmacokinetic Model Building

NONMEM analysis was first performed to fit the blood concentration *versus* time profile of GlySar using a two-compartment PK model. The expanded model, including CSF, was a three-compartment model as shown in Fig. 1a and the estimated PK parameters of GlySar are listed in Table II. Since our laboratory maintains both wild-type and PEPT2 knockout mice, we were able to study the distribution kinetics and estimate the clearance mediated by passive diffusion (CL_{diff}), bulk clearance mediated by CSF bulk flow (CL_{bulk}), and active clearance mediated by PEPT2 (CL_{active}). The total CSF efflux CL ($CL_{CSF\ efflux}$), which equals the sum of CL_{diff}, CL_{bulk}, and CL_{active}, was 4.3-fold higher for wild-type mice compared to PEPT2 knockout mice, demonstrating that PEPT2 plays an important role as an efflux pump in brain. Based on the estimates, it seems that 77% of $CL_{CSF\ efflux}$ is mediated by CL_{active} (i.e., by PEPT2) and the remaining 23% is mediated by CL_{diff} and CL_{bulk}. In addition, the estimated CL_s values of GlySar for wild-type and PEPT2 knock- out mouse were 0.239 and 0.447 ml/min, respectively, which are similar to the results from non-compartmental analysis (Table I). The V_{ss} values for wild-type (9.52 ml) and PEPT2 knockout mouse (14.2 ml) were also similar to the ones observed from non-compartmental analysis. Therefore, it seems that both the WinNonlin and NONMEM analyses agree on the estimation of pharmacokinetic parameters. The three-compartment model also includes inter-subject variability (% CV) on volume of central compartment (V_c, 5.9%), CL_{diff} (36.9%) and CL_s (1.4%) for PEPT2 knockout mice, and V_c (3.8%) and CL_s (2.1%) for wild-type mice.

A four-compartment model was subsequently developed by adding kidney as a separate compartment (Fig. 1b and Table III). The values of CL_{diff} and CL_{bulk} were fixed in the four-compartment model based on the parameter estimates from the previous three-compartment model. Since GlySar is completely eliminated by the kidney, this organ was regarded as the sole eliminating compartment in the four-compartment model. CL_S was almost 2-fold higher for PEPT2 knockout mice compared to wild-type animals, and this is consistent with the results from the three-compartment model. The other estimated parameters of V_c, V_p, V_{CSF}, CL_{active}, and Q are very similar between the three-compartment (Table II) and four-compartment (Table III) models, which demonstrates the robustness of our model. The rate constant K_{14} was calculated as $K_{14}=\frac{CL_S}{V_c}$ and the values were 0.0623 min^{-1} for wild-type mouse and 0.0945 min^{-1} for knockout mouse.

NIH-PA Author Manuscript

NIH-PA Author Manuscript

NIH-PA Author Manuscript

Final Model Validation

Basic goodness-of-fit plots for the final four-compartment model are displayed in Fig. 3. Predicted concentrations of GlySar were highly correlated with observed concentrations in all the blood, CSF and kidney compartments. There were no obvious patterns in the residual plots and the residuals were randomly distributed along the zero line.

The final model was further evaluated using a nonparametric bootstrap analysis. Among 1,000 independent runs, 929 and 968 runs were successfully minimized for wild-type and knockout mice respectively. Median estimates and 90% bootstrap confidence intervals of the final model parameters are shown in Table IV. NONMEM estimates were very similar to median values of the bootstrap estimates and were inside of bootstrap confidence intervals (Table III vs Table IV), indicating there was no significant bias in the NONMEM parameter estimates. Based on the confidence intervals, V_p and CL_S were significantly different between wild-type and knockout mice, as was $CL_{CSF\ efflux}$, since the confidence interval for CL_{active} does not include zero for wild-type mice.

Visual predictive check plots are shown in Fig. 4 as an additional validation method. It seems that the final model well describes the GlySar concentration-time profiles in the blood, CSF and kidney compartments. Moreover, the 5th and 95th percentiles of simulated results were able to cover almost all the observed data.

DISCUSSION

In the present study, a four-compartment PK model was successfully developed to define the distribution and elimination kinetics of a PEPT2 substrate, GlySar, at the BCSFB. Due to the availability of PEPT2 knockout mice, we were able to quantitatively predict, for the first time, the significance of PEPT2 in the efflux kinetics of a PEPT2 substrate at the blood-CSF interface. In this study, we demonstrated that: 1) the distribution of GlySar in blood, CSF and kidney using nonlinear mixed effects modeling approach is best described by a four compartment model; 2) PEPT2 is responsible for 77% of the total CSF efflux of GlySar at the BCSFB with the remaining 23% being mediated by passive diffusion and CSF bulk flow; and 3) the elimination of GlySar was increased by almost 2-fold in the absence of PEPT2 in knockout mice.

CSF is used to predict the extent of CNS penetration of drug molecules since it is easier to collect and analyze compared to other tissues of the brain, and because of ethical constraints in human studies. Drug concentrations in CSF are especially important when the drug target is close to the ventricles, ependyma and leptomeninges, such as in meningitis (24). The CSF is primarily formed in the choroid plexuses and secreted out of the ventricles into the subarachnoid space. Due to the nature of CSF production and bulk flow, the concentration of compounds that are either produced endogenously in brain or passively diffused from blood to brain are low in CSF (1). There are also other regulatory mechanisms that can influence drug exchange across the BCSFB such as the tight junctions of choroid plexus, metabolism of drugs at the BCSFB, and the inwardly- or outwardly-directed movement of drug molecules by transport proteins (1). It has been shown that the morphology of choroid plexus was not changed in PEPT2 knockout mice (21). Therefore, we were able to assume that CL_{diff} is the same for both wild-type mice and PEPT2 knockout animals. In addition, GlySar is resistant to hydrolysis and excreted from the body in intact form (25). Thus, metabolic clearance at the BCSFB was assumed to be zero for GlySar. Based on these assumptions, we were able to construct a model that quantitatively separates the three components contributing to the efflux of GlySar at the BCSFB (i.e., CL_{diff}, CL_{bulk}, and CL_{active}).

NIH-PA Author Manuscript

NIH-PA Author Manuscript

NIH-PA Author Manuscript

To our knowledge, there are no other transporters involved in GlySar uptake into choroid plexus except PEPT2. GlySar may also be transported by PEPT1, PHT1 and PHT2, but there is no molecular or functional evidence to support these transporters having a role in peptide transport systems at the BCSFB (9). In an isolated choroid plexus study, GlySar uptake was very low in PEPT2 knockout mice (almost 10-fold lower compared to wild-type animals), which demonstrates that no other transporters were significantly involved in GlySar uptake into choroid plexus (13). When uptake study was performed using choroid plexus epithelial cells in primary culture, GlySar uptake was significantly inhibited by dipeptides and not L-histidine, ruling out the possibility of other transporters participating in GlySar uptake at the apical membrane (14). At the basolateral membrane, on the other hand, a low affinity uptake process was observed, but the molecular properties of this transporter have not yet been elucidated. Compared to the apical-to-basal transport of GlySar, the reverse transport was very small. Based on this information about di/tripeptide transport mechanisms at the BCSFB, CL_{in} was approximated as CL_{diff}, $CL_{CSF\ efflux}$ was simplified as the combination of CL_{diff}, CL_{bulk} and CL_{active}, and CL_{active} was regarded as only being mediated by PEPT2 in our model.

The quantitative analysis of efflux mechanisms in the brain is meaningful in that the dose of CNS drugs can be adjusted based on expression levels of relevant transporters. The PEPT2 gene is known to be polymorphically expressed in humans with single nucleotide polymorphisms. For example, the genetic variant R57H of PEPT2 shows a complete loss of transport activity (26,27). Based on our estimation that PEPT2 mediates 77% of CSF efflux kinetics for GlySar, we expect the concentrations of this dipeptide to be 4.3-fold greater in CSF during gene deletion. In a previous study, it was shown that CSF-to-blood concentration ratios of GlySar were 4.5-fold higher for PEPT2 null mice compared to wild-type animals (14). Other studies in our laboratory demonstrated that PEPT2 null mice exhibited 6- and 8-fold greater CSF-to-blood concentration ratios for the PEPT2 substrate, cefadroxil and carnosine, respectively (15,28). Additionally, when dose–response studies were performed for L-kyotorphin (L-KTP), an endogenous analgesic neuropeptide and PEPT2 substrate, the ED50 of L-KTP in PEPT2 null mice was five times smaller than in wild-type mice (29). These findings are in agreement with our present results and suggest that dose adjustments for PEPT2 substrate drugs would be needed for brain drug delivery in patients whose PEPT2 function is disrupted.

It would be valuable if we could extrapolate these findings in mouse to human. PEPT2 is expressed in mouse astrocytes, ependymal cells and choroid plexus epithelial cells of brain (9), which forms BCSFB, whereas no evidence of PEPT2 expression at the BBB has been reported. Compared to BBB, little is known about the expression levels of transporters at the BCSFB in human, especially for PEPT2. However, peptide transporters including PEPT2 are known to have high homology (about 80%) and similarities in driving forces, substrate specificity and affinity between mouse and human (3,10-12). If it is further elucidated that both species exhibit similar proton gradients across the membrane and similar expression levels of PEPT2 at the BCSFB, then inter-individual differences in CSF pharmacokinetics of peptide-like drugs, due to PEPT2, could also be simulated in humans.

It has been reported that drug transport systems at the BCSFB are altered in CNS diseases, and these alterations may be associated with morphological and/or functional changes of transport proteins. With respect to morphological changes, alterations of choroid plexus microvilli, severe vacuolization, mitochondria alterations and disruption of tight junction complexes have been reported during CNS inflammatory diseases (2,30-32). With respect to functional changes, several reports have shown that the altered function of transport proteins during CNS diseases contributes to changes in the pharmacokinetics of drugs in brain. For example, the active clearance of organic anions in the choroid plexus was strongly impaired

NIH-PA Author Manuscript

NIH-PA Author Manuscript

NIH-PA Author Manuscript

by exposure to inflammatory stimuli (33). It has also been reported that the uptake of benzylpenicillin in choroid plexus was reduced and CSF levels was increased in an experimental meningitis model (33-35). These changes can disrupt both the diffusion clearance and active clearance of drugs at BCSFB in our model. Therefore, future studies should be directed at investigating quantitatively any changes in efflux mechanisms during CNS inflammatory diseases.

In addition to CSF, there were differences of GlySar concentrations in the kidney of wild-type and PEPT2 knockout mice, which we successfully incorporated into a four-compartment model. PEPT2 is highly expressed in the apical membrane of renal proximal tubular epithelium and plays an important role in the reabsorption of small peptides and peptide-like drugs (8-10). GlySar is only renally excreted and PEPT2 is involved in the renal elimination of Glysar PEPT1 is also known to be involved in the elimination, especially in the reabsorption of peptide-like drugs, but its contribution is relatively minor compared to PEPT2. It has been previously reported that PEPT2 is responsible for 86% of the reabsorption of GlySar and PEPT1 is responsible for only 14% of the reabsorption (14). The model with bootstrap dataset estimated CL_S values of 0.237 and 0.453 in wild-type and PEPT2 knockout mice, respectively (Table IV), showing a statistically significant (1.9 fold) difference between the genotypes ($p < 0.05$). CL_S in four-compartment model describes clearance of drug from the blood compartment and, therefore, it reflects the systemic clearance. The predicted value of CL_S in four-compartment model (Table III) was very similar to those value estimated from the non-compartment (Table I) and the three-compartment model (Table II). Gene deletion of PEPT2 in knockout mouse disrupts reabsorption of GlySar at the apical membrane of renal epithelium, which eventually results in low concentration of GlySar in blood. It seems that the low blood concentration was then reflected as high value of CL_S in knockout mouse. Since GlySar is not actively secreted, has negligible protein binding and golumerular filtration rate is the same for both wild-type and PEPT2 knockout mice (14,15), the difference in CL_S between wild-type and knockout animal may not be attributable to filtration and secretion at the basolateral membrane of renal epithelium.

Peripheral volume (V_p) also shows a 1.6-fold difference in wild-type *versus* PEPT2 knockout animals in the final model (Tables III and IV). From the model, peripheral volume is the sum of apparent tissue volumes, which can be expressed as $V_p = \sum V_t \frac{f_u}{f_{u,t}}$, where V_t is the apparent tissue volume, f_u is the fraction unbound in blood and $f_{u,t}$ is the fraction unbound in tissue. GlySar has negligible protein binding in plasma (14) and, therefore, differences in peripheral volume between wild-type and PEPT2 knockout mice may be mediated by changes in $f_{u,t}$. PEPT2 is not only expressed in choroid plexus and kidney, but it is also expressed in other tissues such as lung and mammary gland (36-38). Therefore, PEPT2 gene deletion in other tissues may affect the increased peripheral volume of GlySar in PEPT2 knockout mice.

CONCLUSION

In conclusion, a population pharmacokinetic model was successfully developed to describe the distribution and elimination kinetics of GlySar, a model PEPT2 substrate, in the blood, CSF and kidney using a nonlinear mixed effects modeling approach. Due to the availability of mice in which the PEPT2 gene is deleted, we were able to quantify the contribution of PEPT2 in the efflux kinetics of GlySar at the BCSFB. In particular, we demonstrated that 77% of the CSF efflux of Glysar was mediated by PEPT2 resulting in approximately 4.3-fold higher CSF concentrations in the PEPT2 knockout mice. Our findings suggest that, given relevant transporter expression levels in tissue, it may be feasible to quantitatively

NIH-PA Author Manuscript

NIH-PA Author Manuscript

NIH-PA Author Manuscript

predict the distribution of CNS drugs at the BCSFB and to use this information accordingly for dose adjustments in clinical therapy. Future studies should investigate changes in the distribution kinetics of peptides/mimetics at the BCSFB in disease states such as meningitis, and the possibility of quantifying the impact of such changes on the CSF efflux of peptide-like drugs using a modeling approach.

Acknowledgments

DISCLOSURES

This work was supported by the National Institutes of Health General Medical Sciences [Grant R01-GM035498] (to D.E.S.). The authors would also like to thank Dr Matt Hutmacher from the Ann Arbor Pharmacometrics Group-A2pg for valuable suggestions for the population PK model development.

References

1. Smith DE, Johanson CE, Keep RF. Peptide and peptide analog transport systems at the blood-CSF barrier. Adv Drug Deliv Rev. 2004; 56(12):1765–91. [PubMed: 15381333]
2. Coisne C, Engelhardt B. Tight junctions in brain barriers during central nervous system inflammation. Antioxid Redox Signal. 2011; 15(5):1285–303. [PubMed: 21338320]
3. Thomas SA, Segal MB. The transport of the anti-HIV drug, 2′,3′-didehydro-3′-deoxythymidine (D4T), across the blood–brain and blood-cerebrospinal fluid barriers. Br J Pharmacol. 1998; 125(1): 49–54. [PubMed: 9776343]
4. Ghersi-Egea JF, Gorevic PD, Ghiso J, Frangione B, Patlak CS, Fenstermacher JD. Fate of cerebrospinal fluid-borne amyloid beta-peptide: rapid clearance into blood and appreciable accumulation by cerebral arteries. J Neurochem. 1996; 67(2):880–3. [PubMed: 8764620]
5. Ghersi-Egea JF, Finnegan W, Chen JL, Fenstermacher JD. Rapid distribution of intraventricularly administered sucrose into cerebrospinal fluid cisterns *via* subarachnoid velae in rat. Neuroscience. 1996; 75(4):1271–88. [PubMed: 8938759]
6. Kusuhara H, Sugiyama Y. Efflux transport systems for organic anions and cations at the blood-CSF barrier. Adv Drug Deliv Rev. 2004; 56(12):1741–63. [PubMed: 15381332]
7. Daniel H, Rubio-Aliaga I. An update on renal peptide transporters. Am J Physiol Ren Physiol. 2003; 284(5):F885–92.
8. Smith DE, Pavlova A, Berger UV, Hediger MA, Yang T, Huang YG, et al. Tubular localization and tissue distribution of peptide transporters in rat kidney. Pharm Res. 1998; 15(8):1244–9. [PubMed: 9706056]
9. Takahashi K, Nakamura N, Terada T, Okano T, Futami T, Saito H, et al. Interaction of beta-lactam antibiotics with H+/peptide cotransporters in rat renal brush-border membranes. J Pharmacol Exp Ther. 1998; 286(2):1037–42. [PubMed: 9694966]
10. Shen H, Smith DE, Yang T, Huang YG, Schnermann JB, Brosius FC 3rd. Localization of PEPT1 and PEPT2 proton-coupled oligopeptide transporter mRNA and protein in rat kidney. Am J Physiol. 1999; 276(5 Pt 2):F658–65. [PubMed: 10330047]
11. Shu C, Shen H, Teuscher NS, Lorenzi PJ, Keep RF, Smith DE. Role of PEPT2 in peptide/mimetic trafficking at the blood-cerebrospinal fluid barrier: studies in rat choroid plexus epithelial cells in primary culture. J Pharmacol Exp Ther. 2002; 301(3):820–9. [PubMed: 12023509]
12. Teuscher NS, Shen H, Shu C, Xiang J, Keep RF, Smith DE. Carnosine uptake in rat choroid plexus primary cell cultures and choroid plexus whole tissue from PEPT2 null mice. J Neurochem. 2004; 89(2):375–82. [PubMed: 15056281]
13. Shen H, Smith DE, Keep RF, Brosius FC 3rd. Immunolocalization of the proton-coupled oligopeptide transporter PEPT2 in developing rat brain. Mol Pharm. 2004; 1(4):248–56. [PubMed: 15981584]
14. Ocheltree SM, Shen H, Hu Y, Keep RF, Smith DE. Role and relevance of peptide transporter 2 (PEPT2) in the kidney and choroid plexus: *in vivo* studies with glycylsarcosine in wild-type and PEPT2 knockout mice. J Pharmacol Exp Ther. 2005; 315(1):240–7. [PubMed: 15987832]

NIH-PA Author Manuscript

NIH-PA Author Manuscript

NIH-PA Author Manuscript

15. Shen H, Ocheltree SM, Hu Y, Keep RF, Smith DE. Impact of genetic knockout of PEPT2 on cefadroxil pharmacokinetics, renal tubular reabsorption, and brain penetration in mice. Drug Metab Dispos. 2007; 35(7):1209–16. [PubMed: 17452417]

16. Hu Y, Shen H, Keep RF, Smith DE. Peptide transporter 2 (PEPT2) expression in brain protects against 5-aminolevulinic acid neurotoxicity. J Neurochem. 2007; 103(5):2058–65. [PubMed: 17854384]

17. Shafer SL, Eisenach JC, Hood DD, Tong C. Cerebrospinal fluid pharmacokinetics and pharmacodynamics of intrathecal neostigmine methylsulfate in humans. Anesthesiology. 1998; 89(5):1074–88. [PubMed: 9821995]

18. Khatri A, Gaber MW, Brundage RC, Naimark MD, Hanna SK, Stewart CF, et al. Effect of radiation on the penetration of irinotecan in rat cerebrospinal fluid. Cancer Chemother Pharmacol. 2010; 68(3):721–31. [PubMed: 21161529]

19. Nalda-Molina R, Dokoumetzidis A, Charkoftaki G, Dimaraki E, Margetis K, Archontaki H, et al. Pharmacokinetics of doripenem in CSF of patients with non-inflamed meninges. J Antimicrob Chemother. 2012; 67(7):1722–9. [PubMed: 22457313]

20. Pfister M, Zhang L, Hammarlund-Udenaes M, Sheiner LB, Gerber CM, Tauber MG, et al. Modeling of transfer kinetics at the serum-cerebrospinal fluid barrier in rabbits with experimental meningitis: application to grepafloxacin. Antimicrob Agents Chemother. 2003; 47(1):138–43. [PubMed: 12499181]

21. Shen H, Smith DE, Keep RF, Xiang J, Brosius FC 3rd. Targeted disruption of the PEPT2 gene markedly reduces dipeptide uptake in choroid plexus. J Biol Chem. 2003; 278(7):4786–91. [PubMed: 12473671]

22. Keep RF, Si X, Shakui P, Ennis SR, Betz AL. Effect of amiloride analogs on DOCA-salt-induced hypertension in rats. Am J Physiol. 1999; 276(6 Pt 2):H2215–20. [PubMed: 10362706]

23. Stroobants S, Gerlach D, Matthes F, Hartmann D, Fogh J, Gieselmann V, et al. Intracerebroventricular enzyme infusion corrects central nervous system pathology and dysfunction in a mouse model of metachromatic leukodystrophy. Hum Mol Genet. 2011; 20(14): 2760–9. [PubMed: 21515587]

24. de Lange EC, Danhof M. Considerations in the use of cerebrospinal fluid pharmacokinetics to predict brain target concentrations in the clinical setting: implications of the barriers between blood and brain. Clin Pharmacokinet. 2002; 41(10):691–703. [PubMed: 12162757]

25. Krzysik BA, Adibi SA. Comparison of metabolism of glycine injected intravenously in free and dipeptide forms. Metabolism. 1979; 28(12):1211–7. [PubMed: 514081]

26. Pinsonneault J, Nielsen CU, Sadee W. Genetic variants of the human H+/dipeptide transporter PEPT2: analysis of haplotype functions. J Pharmacol Exp Ther. 2004; 311(3):1088–96. [PubMed: 15282265]

27. Terada T, Irie M, Okuda M, Inui K. Genetic variant Arg57His in human H+/peptide cotransporter 2 causes a complete loss of transport function. Biochem Biophys Res Commun. 2004; 316(2):416–20. [PubMed: 15020234]

28. Kamal MA, Jiang H, Hu Y, Keep RF, Smith DE. Influence of genetic knockout of Pept2 on the *in vivo* disposition of endogenous and exogenous carnosine in wild-type and Pept2 null mice. Am J Physiol Regul Integr Comp Physiol. 2009; 296(4):R986–91. [PubMed: 19225147]

29. Jiang H, Hu Y, Keep RF, Smith DE. Enhanced antinociceptive response to intracerebroventricular kyotorphin in Pept2 null mice. J Neurochem. 2009; 109(5):1536–43. [PubMed: 19383084]

30. Endo H, Sasaki K, Tonosaki A, Kayama T. Three-dimensional and ultrastructural ICAM-1 distribution in the choroid plexus, arachnoid membrane and dural sinus of inflammatory rats induced by LPS injection in the lateral ventricles. Brain Res. 1998; 793(1–2):297–301. [PubMed: 9630685]

31. Johanson CE, Palm DE, Primiano MJ, McMillan PN, Chan P, Knuckey NW, et al. Choroid plexus recovery after transient fore-brain ischemia: role of growth factors and other repair mechanisms. Cell Mol Neurobiol. 2000; 20(2):197–216. [PubMed: 10696510]

32. Engelhardt B, Wolburg-Buchholz K, Wolburg H. Involvement of the choroid plexus in central nervous system inflammation. Microsc Res Tech. 2001; 52(1):112–29. [PubMed: 11135454]

NIH-PA Author Manuscript

NIH-PA Author Manuscript

NIH-PA Author Manuscript

33. Strazielle N, Khuth ST, Murat A, Chalon A, Giraudon P, Belin MF, et al. Pro-inflammatory cytokines modulate matrix metalloproteinase secretion and organic anion transport at the blood-cerebrospinal fluid barrier. J Neuropathol Exp Neurol. 2003; 62(12):1254–64. [PubMed: 14692701]

34. Spector R, Lorenzo AV. Inhibition of penicillin transport from the cerebrospinal fluid after intracisternal inoculation of bacteria. J Clin Invest. 1974; 54(2):316–25. [PubMed: 4546548]

35. Han H, Kim SG, Lee MG, Shim CK, Chung SJ. Mechanism of the reduced elimination clearance of benzylpenicillin from cerebrospinal fluid in rats with intracisternal administration of lipopolysaccharide. Drug Metab Dispos. 2002; 30(11):1214–20. [PubMed: 12386127]

36. Berger UV, Hediger MA. Distribution of peptide transporter PEPT2 mRNA in the rat nervous system. Anat Embryol (Berl). 1999; 199(5):439–49. [PubMed: 10221455]

37. Meredith D, Boyd CA. Structure and function of eukaryotic peptide transporters. Cell Mol Life Sci. 2000; 57(5):754–78. [PubMed: 10892342]

38. Groneberg DA, Fischer A, Chung KF, Daniel H. Molecular mechanisms of pulmonary peptidomimetic drug and peptide transport. Am J Respir Cell Mol Biol. 2004; 30(3):251–60. [PubMed: 14969997]

ABBREVIATIONS

ABC	ATP–binding cassette
BCSFB	blood-cerebrospinal fluid barrier
CNS	central nervous system
CSF	cerebrospinal fluid
GlySar	glycylsarcosine
IPRED	individual model predictions
MRT	mean residence time
NONMEM	nonlinear mixed effects modeling
OFV	objective function value
PEPT2	peptide transporter 2
PK	pharmacokinetic
POT	proton-coupled oligopeptide transporter
PRED	population model predictions
RSE	relative standard error
SLC	solute carrier
WRES	weighted residuals

NIH-PA Author Manuscript

NIH-PA Author Manuscript

NIH-PA Author Manuscript

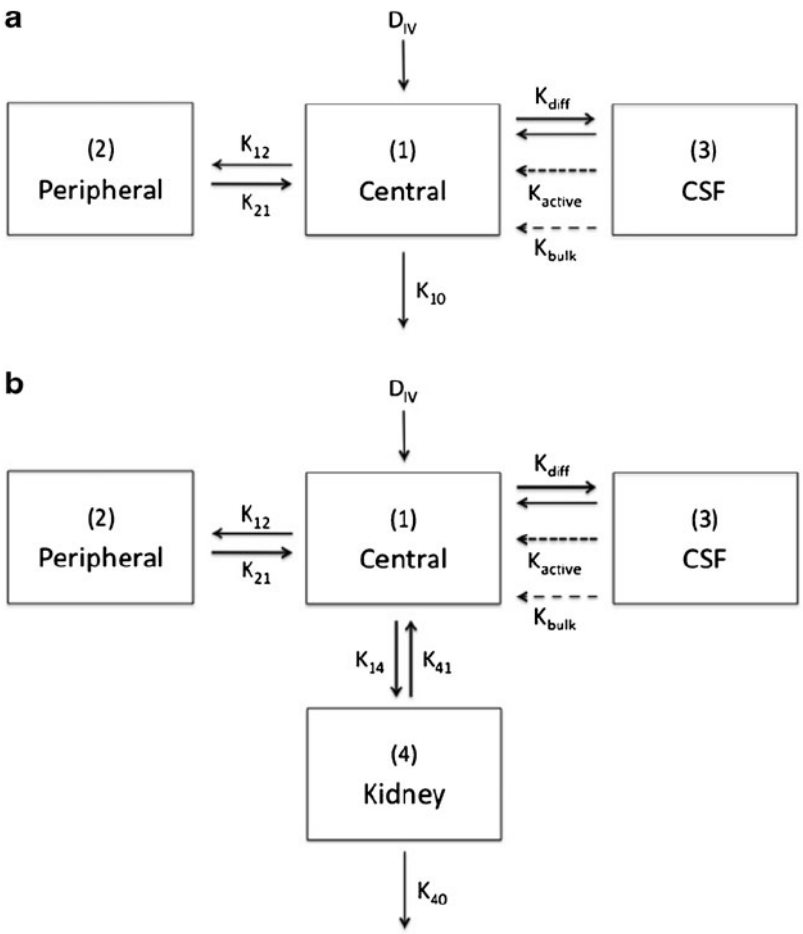

Fig. 1.

Schematic representation of three- (**a**) and four-compartment (**b**) models to simultaneously describe the blood, CSF, and kidney data. Drug molecules are only eliminated by the kidney. K_{diff}, K_{bulk} and K_{active} are distribution rate constants describing GlySar transport between blood and CSF mediated by passive diffusion, CSF bulk flow and PEPT2, respectively.

NIH-PA Author Manuscript
NIH-PA Author Manuscript
NIH-PA Author Manuscript

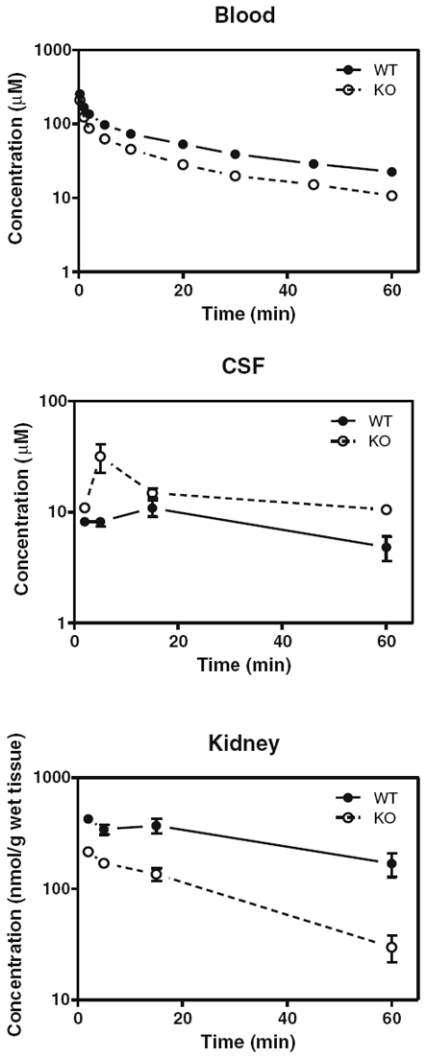

Fig. 2.

GlySar concentration *versus* time plots for the blood, CSF and kidney compartments. *Closed circles* represent the data from wild-type mice (WT) and *open circles* represent the data from PEPT2 knockout mice (KO). The figures were adapted from a previous publication (14).

NIH-PA Author Manuscript

NIH-PA Author Manuscript

NIH-PA Author Manuscript

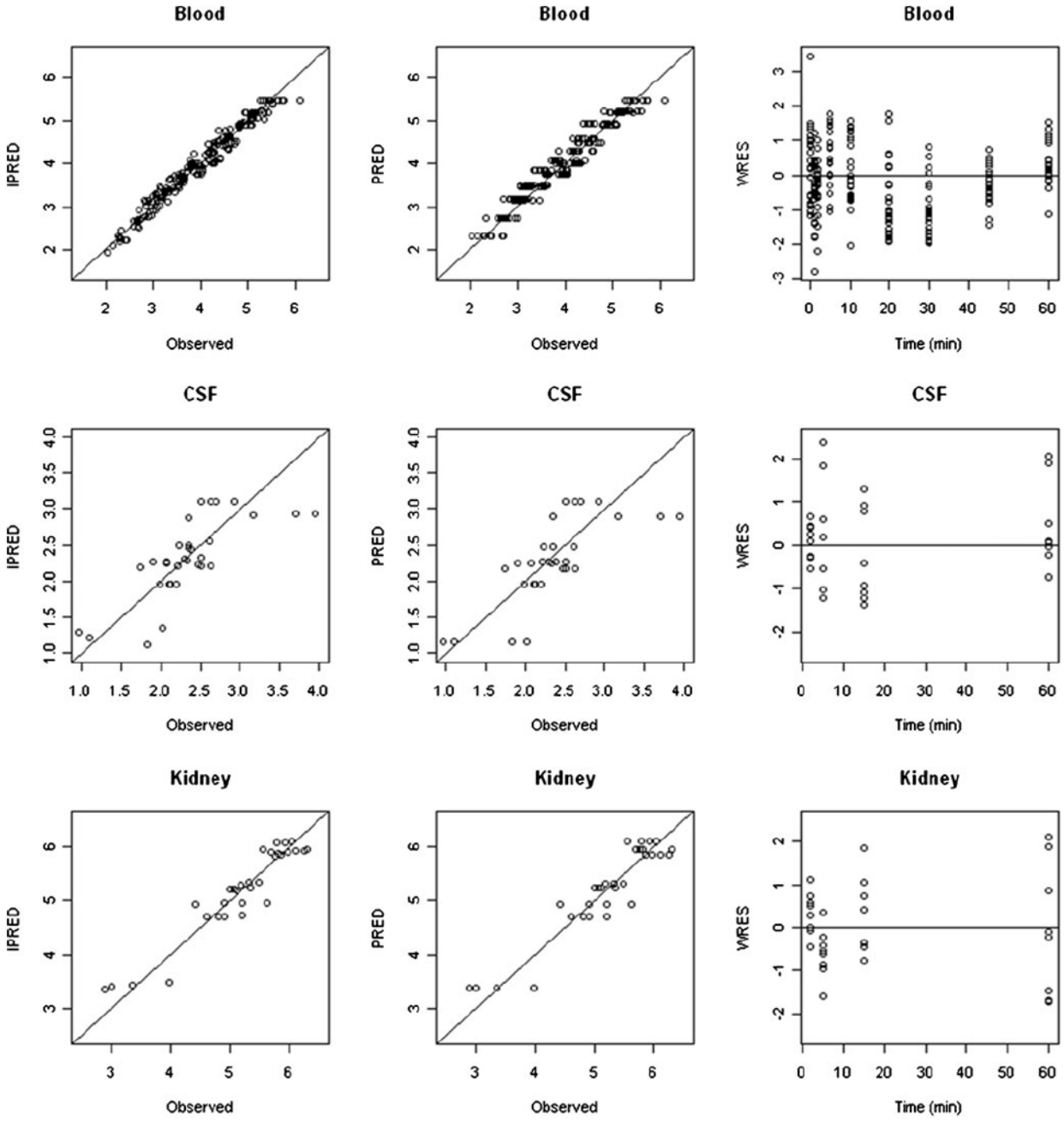

Fig. 3.

Goodness-of-fit plots for the final pharmacokinetic model. Wild-type and knockout animal data were combined. *Solid lines* represent the identity line. *PRED* population model predictions; *IPRED* individual model predictions; *WRES* weighted residuals.

NIH-PA Author Manuscript

NIH-PA Author Manuscript

NIH-PA Author Manuscript

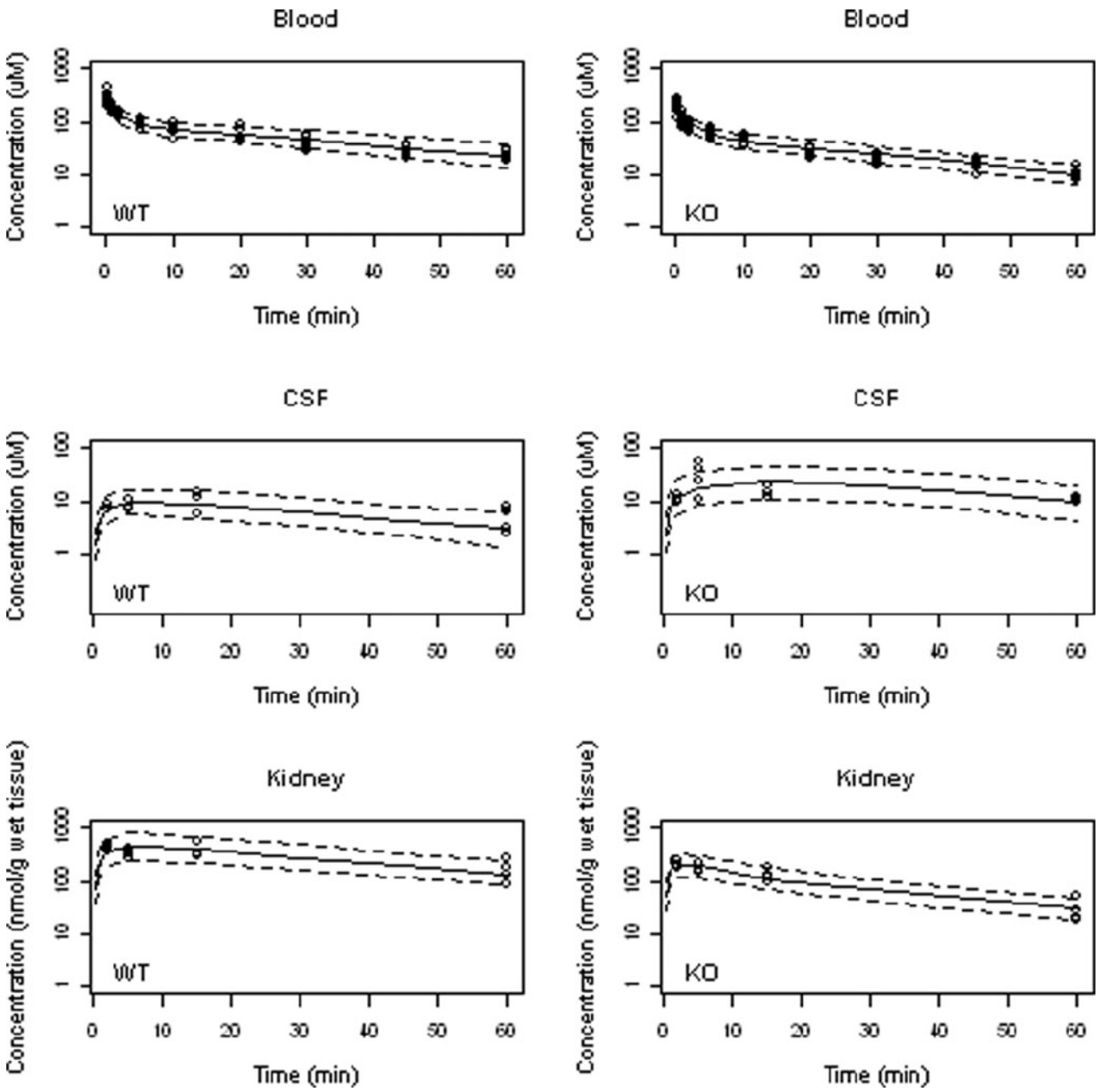

Fig. 4.

Simulated concentration-time profiles of 1,000 subjects in the blood, CSF and kidney compartments of wild-type (WT) and knockout (KO) mice. Simulations are based on the final model. The circles represent the observed data in mice. *Dashed lines* depict the 5th and 95th percentiles and *solid lines* depict the median values of simulated data sets.

NIH-PA Author Manuscript

NIH-PA Author Manuscript

NIH-PA Author Manuscript

Table I

Non-compartmental Analysis of GlySar Blood Concentrations in Wild-Type and PEPT2 Knockout Mice

Parameter	Wild-type mice	Knockout mice
Vss (ml)	10.7 ± 2.3	15.6 ± 2.6***
CL_s (ml/min)	0.235 ± 0.034	0.438 ± 0.074***
$t_{1/2}$ (min)	36.1 ± 9.5	30.8 ± 5.7
MRT (min)	45.8 ± 11.3	36.1 ± 5.7*
$AUC_{blood,\ 0\text{-}tlast}$ (min • nmol/ml)	3149 ± 500	1848 ± 285***
$AUC_{CSF,\ 0\text{-}tlast}$ (min • nmol/ml)[a]	482	880
$AUC_{CSF,\ 0\text{-}tlast}/AUC_{blood,\ 0\text{-}tlast}$	0.153	0.476

* $p < 0.05$

*** $p < 0.001$

[a] AUC in the CSF compartment was estimated using mean data since every sample was collected from a different animal

NIH-PA Author Manuscript
NIH-PA Author Manuscript
NIH-PA Author Manuscript

Table II

Parameter Estimates for the Three-Compartment Model of Glysar in Wild-Type and PEPT2 Knockout Mice

Parameters	Wild-type mice		Knockout mice	
	Estimate	RSE (%)	Estimate	RSE (%)
Distribution parameters				
V_c (ml)	3.83	10.1	4.93	7.40
V_p (ml)	5.67	9.07	9.27	4.79
V_{CSF} (ml)	0.0230	14.9	0.0112	11.4
V_{ss} (ml)[a]	9.52	–	14.2	–
Q (ml/min)[b]	1.36	23.2	1.66	14.8
CL_{diff} (μl/min)	0.509	–	0.509	19.3
CL_{bulk} (μl/min)[c]	0.325	–	0.325	–
CL_{active} (μl/min)	2.73	22.7	–	–
$CL_{CSF\ efflux}$ (μl/min)	3.564	–	0.834	–
CL_s (ml/min)[d]	0.239	4.35	0.447	3.67
$t_{1/2}$ (min)[e]	27.6	–	22.0	–
Inter-subject variability[f] (CV%)				
V_c	3.82	16.9	5.94	42.8
$CL_{diffusion}$	–	–	36.9	44.2
CL_s	2.12	40.0	1.39	42.4
Residual variability[f] (CV%)				
Plasma	20.3	8.38	42.3	8.79
CSF	39.4	14.7	23.1	54.1

[a] V_{ss} was calculated as sum of V_C, V_p, and V_{CSF}

[b] $Q = K_{12}V_c = K_{21}V_p$

[c] CL_{bulk} was fixed based on the literature value (22)

[d] $CL_s = K_{10}V_c$

[e] $t_{1/2}$ was calculated as $t_{1/2} = \ln 2 \times \frac{V_{ss}}{CL_s}$

[f] Inter-subject and residual variabilities were expressed as coefficient of variation (CV%)

NIH-PA Author Manuscript
NIH-PA Author Manuscript
NIH-PA Author Manuscript

Table III

Parameter Estimates for the Four-Compartment Model of Glysar in Wild-Type and PEPT2 Knockout Mice

Parameters	Wild-type mice		Knockout mice	
	Estimate	RSE (%)	Estimate	RSE (%)
Distribution parameters				
V_c (ml)	3.79	9.71	4.75	7.40
V_p (ml)	5.75	8.87	9.18	4.78
V_{CSF} (ml)	0.0229	18.3	0.0112	19.9
V_{kidney} (ml)	0.199	35.1	0.408	26.0
V_{ss} (ml)[a]	9.76	–	14.3	–
Q (ml/min)[b]	1.39	22.1	1.78	42.2
CL_{diff} (μl/min)	0.509	–	0.509	–
CL_{bulk} (μl/min)[c]	0.325	–	0.325	–
CL_{active} (μl/min)	2.76	29.2	–	–
$CL_{CSF\ efflux}$ (μl/min)	3.594	–	0.834	–
CL_S(ml/min)[d]	0.236	6.06	0.449	3.79
K_{40}(min^{-1})	0.220	43.6	0.405	32.3
$t_{1/2}$ (min)[e]	28.7	–	22.1	–
Inter-subject variability[f](CV%)				
V_c	2.36	32.4	1.35	43.2
CL_S	2.66	40.3	5.54	44.9
Residual variability[f](CV%)				
Plasma	20.2	8.04	17.9	8.85
CSF	36.2	17.4	31.5	16.5
Kidney	39.1	15.0	55.0	19.5

[a] V_{ss} was calculated as sum of V_C, V_p, V_{CSF} and V_{kidney}

[b] $Q = K_{12}V_C = K_{21}V_p$

[c] CL_{bulk} was fixed based on the literature value (22)

[d] $CL_S = K_{14}V_C$

[e] $t_{1/2}$ was calculated as $t_{1/2} = \ln 2 \times \frac{V_{ss}}{CL_{14}}$

[f] Inter-subject and residual variabilities were expressed as coefficient of variation (CV%)

NIH-PA Author Manuscript

NIH-PA Author Manuscript

NIH-PA Author Manuscript

Table IV

Parameter Confidence Intervals (CI) for the Finalized Four-Compartment Model, Estimated by Bootstrap Method

Parameters	Wild-type mice		Knockout mice	
	Median	90% CI	Median	90% CI
V_c (ml)	3.86	3.16–4.69	4.94	4.23–6.21
V_p (ml)	5.87	4.98–7.24	9.35	8.49–11.6
V_{CSF} (ml)	0.0226	0.016–0.0312	0.0111	0.00676–0.0163
V_{kidney} (ml)	0.201	0.0725–0.301	0.378	0.166–0.653
Q (ml/min)	1.33	0.485–1.84	1.76	0.771–2.27
CL_{diff} (μl/min)	0.509	–	0.509	–
CL_{bulk} (μl/min)[a]	0.325	–	0.325	–
CL_{active} (μl/min)	2.82	1.84–4.11	–	–
$CL_{CSF\ efflux}$ (μl/min)	3.654	–	0.834	–
CL_S(ml/min)	0.237	0.205–0.255	0.453	0.419–0.492
K_{40}(min^{-1})	0.216	0.123–0.446	0.458	0.244–0.993

[a] CL_{bulk} was fixed based on the literature value (22)